

# **CVD Synthesis of Single Crystal Diamond Films on Silicon Substrates Without Seeding**

**Randell Mills\***

**Jayasree Sankar**

**Paresh Ray**

**Bala Dhandapani**

**Jiliang He**

BlackLight Power, Inc.  
493 Old Trenton Road  
Cranbury, NJ 08512

Single crystal diamond films were synthesized on silicon substrates for the first time without diamond seeding by a microwave plasma reaction of a mixture of 10-30% hydrogen, 90-70% helium, and 1-10%  $CH_4$ . The films were characterized by time of flight secondary ion mass spectroscopy (ToF-SIMS), X-ray photoelectron spectroscopy (XPS), Raman spectroscopy, and X-ray diffraction (XRD). It is proposed that  $He^+$  served as a catalyst with atomic hydrogen to form an energetic plasma. The average hydrogen atom temperature was measured to be 180-210 eV versus  $\approx 3$  eV for pure hydrogen. The electron temperature  $T_e$  for helium-hydrogen was 28,000 K compared to 6800 K for pure helium. Bombardment of the carbon surface by highly energetic hydrogen formed by the catalysis reaction may play a role in the formation of diamond. Then, by this novel pathway, the relevance of the C-H-O tie line is eliminated along with other stringent conditions and complicated and inefficient techniques which limit broad application of the versatility and superiority of diamond thin film technology.

\* Phone: 609-490-1090; Fax: 609-490-1066; E-mail: [rmills@blacklightpower.com](mailto:rmills@blacklightpower.com)

## I. INTRODUCTION

Diamond has some of the most extreme physical properties of any material such as outstanding mechanical strength, optical transparency, high thermal conductivity, high electron mobility, and unique chemical properties [1]. Thus, a variety of possible applications are envisioned for diamond materials. Yet, its practical use in applications has been limited due to its scarcity, expense, and immalleability. The development of techniques for depositing thin films of synthetic diamonds on a variety of substrates has enabled the exploitation of diamond's superlative properties in many new and exciting applications. These include cutting tools, thermal management of integrated circuits, optical windows, high temperature electronics, surface acoustic wave (SAW) filters, field emission displays, electrochemical sensors, composite reinforcement, microchemical devices and sensors, and particle detectors [1]. But, the fundamental impediment facing the technology at the present is insufficient growth rate of high-quality diamond.

Synthetic diamond was initially commercially produced as single crystals using the so-called high-pressure high-temperature (HPHT) growth technique [1] wherein graphite is compressed in a hydraulic press to tens of thousands of atmospheres, heated to over 2000 K, and left until diamond crystallizes. Recent novel HPHT methods which have been largely unsuccessful, except for the production of nanocrystals by Orwa et. al. [2], are based on attempts to use high energy ion implantation to bury carbon deep in metals or fused silica to take advantage of the large confining pressures there. More versatile thin films have been produced by an addition-of-one-atom-at-a-time approach using chemical vapor deposition (CVD) techniques. All CVD techniques for producing diamond films require activation of the gaseous carbon-containing precursor molecules. To promote diamond over graphite growth, the precursor gas is usually  $CH_4$  that is diluted in excess hydrogen that is typically 99% of the reactant mixture, and the temperature of the substrate is usually maintained in excess of 700°C. Activation may be achieved thermally using a hot filament, gas discharge such as DC, RF, or microwave discharges, or a combustion flame such as an oxyacetylene torch [1].

Although the mechanism of diamond growth on a seed of diamond is still somewhat of a mystery, it is believed to be based on the extraction of  $H$  of a  $CH$  terminal bond to form a dangling carbon center to which  $CH_3$  reacts. A carbon-carbon bond forms between adjacent methyl groups, and the hydrogen is gradually extracted, probably by  $H$  forming  $H_2$ . The further preferential degradation of graphitic carbon over diamond carbon by hydrogen permits diamond growth [1].  $H$  may also be required to decrease the concentration of gas phase unsaturated hydrocarbons.

More recent advances of diamond formation have been towards developing methods to grow diamond at low temperatures ( $< 500^\circ\text{C}$  rather than  $700^\circ\text{C}$ ) such that diamond films can be grown on a wider range of substrate materials of commercial importance with low melting points such as plastics, aluminum, some glasses, nickel, steel and electronics materials such as  $GaAs$ . Many gas mixtures have been investigated to achieve this goal including ones containing some halogens, presumably substituting for the role played by  $H$  [3]. More common mixtures have different combinations of  $H_2$ ,  $CH_4$ ,  $O_2$ ,  $CO_2$ , and  $CO$  [3]. Quite successful diamond film growth has been achieved at temperatures as low as  $180^\circ\text{C}$  using gas mixtures of  $CH_4$  mixed with  $CO_2$  or  $CO$  in microwave plasma deposition reactors wherein an optimal rate is obtained when the gas ratio is about 50/50%. Although the concentration of  $H_2$  in the activated gas mixture is approximately half that seen in the  $CH_4/H_2$  mixtures [4], the  $CO_2-CH_4$  and  $CO-CH_4$  systems are unique in that hydrogen is low compared to the excess needed in other systems presumably because oxygen species such as  $O_2$ ,  $O$ , and  $OH$  in the  $CO_2-CH_4$  and  $CO-CH_4$ -system plasmas perform the same role as  $H$  in the  $CH_4-H_2$ -system plasmas. Recent molecular beam mass spectroscopy investigations of the  $CO_2-CH_4$  system indicate the incorporation of  $CH_3$  at a dangling carbon bond is the most probable mechanism as in the case of the  $CH_4-H_2$  system. However, the species that extracts  $H$  may not be an oxygen species. Rather,  $CO$  may activate the surface by extracting a terminating  $H$  [5].

Empirically it is known that only narrow set of ratios of  $O$ ,  $C$ , and  $H$  result in diamond formation. Using the combined data from over 70 diamond deposition experiments, Bachmann et al. produced a  $C-H-O$

phase diagram for diamond deposition which showed that low pressure diamond synthesis is only possible within a very narrow well-defined domain centered on a line called the  $C-H-O$  tie line [6-7]. A consequence of this analysis was that the exact nature of the plasma gases was unimportant for most CVD processes; rather, the relative ratios of  $O$ ,  $C$ , and  $H$  controlled the deposition.

It was previously reported that a novel highly stable surface coating  $SiH$  which comprised high binding energy hydride ions was synthesized by microwave plasma reaction of mixture of silane, hydrogen, and helium wherein it was proposed that  $He^+$  served as a catalyst with atomic hydrogen to form the highly stable hydride ions [8]. The novel silicon hydride was identified by time of flight secondary ion mass spectroscopy (ToF-SIMS) and X-ray photoelectron spectroscopy (XPS). ToF-SIMS identified the coatings as hydride by the large  $SiH^+$  peak in the positive spectrum and the dominant  $H^-$  in the negative spectrum. XPS identified the  $H$  content of the  $SiH$  coatings as hydride ions corresponding to peaks at 11, 43, and 55 eV with no corresponding primary element peaks. The silicon hydride surface was remarkably stable in air for long duration exposure as shown by XPS.

In the quest for low temperature diamond synthesis,  $CH_4$  was substituted for  $SiH_4$  in the helium-hydrogen microwave reaction which formed novel  $SiH$ . We report for the first time the deposition of single crystal diamond films on silicon-wafers by a helium-hydrogen- $CH_4$  (90-70/10-30/1-10%) microwave plasma maintained with an Evenson cavity without diamond seeding or abrasion that provides seed crystals [9]. After the plasma processing reaction, the surface was characterized by ToF-SIMS, XPS, Raman spectroscopy, and X-ray diffraction (XRD). In order to understand the role of the helium-hydrogen plasma, it was characterized by recording the line broadening of the 656.3 nm Balmer  $\alpha$  line to determine the excited hydrogen atom energy. The electron temperature  $T_e$  was also measured using the ratio of the intensity  $I$  of two lines in two quantum states such as the ratio  $I(He\ 501.6\ nm\ line)/I(He\ 492.2\ nm\ line)$ .

## II. EXPERIMENTAL

## Synthesis

Diamond films were grown on silicon wafer substrates by their exposure to a low pressure  $He/H_2/CH_4$  microwave plasma. The experimental set up comprising a microwave discharge cell operated under flow conditions is shown in Figure 1. A silicon wafer substrate (0.5 X 0.5 X 0.05 cm, Silicon Quest International, silicon (100), boron doped) cleaned by heating to 700°C under vacuum was placed about 2 cm off center inside of a quartz tube (1.2 cm in diameter by 25 cm long) with vacuum valves at both ends. The tube was center-fitted with an Opthos coaxial microwave cavity (Evenson cavity) and connected to the gas/vacuum line. The quartz tube and vacuum line were evacuated for 2 hours to remove any trace moisture or oxygen and residual gases. A premixed  $He$  (90-70%)/ $H_2$  (10-30%)/ $CH_4$  (1-10%) plasma gas was flowed through the quartz tube at a total pressure of 1.5 Torr maintained with a gas flow rate of 40 sccm controlled by a mass flow controller with a readout. The cell pressure was monitored by an absolute pressure gauge. The microwave generator shown in Figure 1 was an Opthos model MPG-4M generator (Frequency: 2450 MHz). The microwave plasma was maintained with a 40 W (forward)/2 W (reflected) power for about 12-16 hrs. The substrate was at the cool edge of the plasma glow region. The wall temperature at this position was about 300°C. A thick (~100  $\mu m$ ) crystalline, shiny coating formed on the substrate and the wall of the quartz reactor. The quartz tube was removed and transferred to a drybox with the samples inside by closing the vacuum valves at both ends and detaching the tube from the vacuum/gas line. The coated silicon wafer substrate was mounted on XPS and ToF-SIMS sample holders under an argon atmosphere in order to prepare samples for the corresponding analyses. Controls for XPS analysis comprised a cleaned commercial silicon wafer (Silicon Quest International, silicon (100), boron doped) and known standards: (a) single crystal diamond, (b) diamond film, (c) glassy carbon, (d) pyrolytic graphite, (e) mineral graphite, and (f) HDLC (hydrogenated diamond-like carbon). The control for ToF-SIMS analysis comprised a cleaned commercial silicon wafer (Silicon Quest International, silicon (100), boron doped). The coated substrate was also sent for Raman analysis (Charles Evans & Associates, Sunnyvale, CA) and XRD analysis (IC Laboratories, Amawalk, NY).

### ToF-SIMS Characterization

A cleaned commercial silicon wafer before and after plasma treatment to form a diamond film coating were characterized using a Physical Electronics TRIFT ToF-SIMS instrument. The primary ion source was a pulsed  $^{69}\text{Ga}^+$  liquid metal source operated at 15 keV. The secondary ions were exacted by a  $\pm 3$  keV (according to the mode) voltage. Three electrostatic analyzers (Triple-Focusing-Time-of-Flight) deflect them in order to compensate for the initial energy dispersion of ions of the same mass. The 400 pA dc current was pulsed at a 5 kHz repetition rate with a 7 ns pulse width. The analyzed area was  $60\mu\text{m} \times 60\mu\text{m}$  and the mass range was 0-1000 AMU. The total ion dose was  $7 \times 10^{11} \text{ ions/cm}^2$ , ensuring static conditions. Charge compensation was performed with a pulsed electron gun operated at 20 eV electron energy. In order to remove surface contaminants and expose a fresh surface for analysis, the samples were sputter-cleaned for 30 s using a  $80\mu\text{m} \times 80\mu\text{m}$  raster, with 600 pA current, resulting in a total ion dose of  $10^{15} \text{ ions/cm}^2$ . Three different regions on each sample of  $60\mu\text{m} \times 60\mu\text{m}$  were analyzed. The positive and negative SIMS spectra were acquired. Representative post sputtering data is reported. The ToF-SIMS data were treated using 'Cadence' software (Physical Electronics), which calculates the mass calibration from well-defined reference peaks.

### XPS Characterization

A series of XPS analyses were made on the samples using a Scienta 300 XPS Spectrometer at Lehigh University, Bethlehem, PA. The fixed analyzer transmission mode and the sweep acquisition mode were used. The Aluminum X-ray incidence angle was  $15^\circ$ . The step energy in the survey scan was  $0.5 \text{ eV}$ , and the step energy in the high resolution scan was  $0.15 \text{ eV}$ . In the survey scan, the time per step was 0.4 seconds, and the number of sweeps was 4. In the high resolution scan, the time per step was 0.3 seconds, and the number of sweeps was 30.  $\text{C } 1s$  at  $284.6 \text{ eV}$  was used as the internal standard.

### Raman Spectroscopy

Experimental and control samples were analyzed by Charles Evans & Associates, Sunnyvale, CA. Raman spectra were obtained with a LABRAM spectrometer (Dilor of Jobin Yvon) with a Spectrum One CCD (charge coupled device) detector (Spex and Jobin Yvon) that was air and Peltier cooled. An Omnicrome HeNe laser (Melles Griot) with the light wavelength of 632.817 nm was used as the excitation source. The spectra were taken at ambient conditions and the samples were placed under a Raman microscope (Olympus BX40). Spectra of the film samples were acquired using the following condition: the laser power at the sample was 4 to 8 mW, the slit width of the monochromator was 100  $\mu\text{m}$  which corresponds to a resolution of 3  $\text{cm}^{-1}$ , the detector exposure time was 20 mins., and 3 scans were averaged.

#### Characterization by X-ray Diffraction (XRD)

The XRD patterns were obtained by IC Laboratories (Amawalk, NY) using a Phillips 547 Diffractometer tuned for  $\text{Cu K}_\alpha$  (1.540590 Å) radiation generated at 45 kV and 35 mA. The sample was scanned from 10 to 100 2-theta ( $2\theta$ ) with a step size of 0.02° and 1 second per step.

#### Balmer $\alpha$ line broadening and $T_e$ measurements

The width of the 656.3 nm Balmer  $\alpha$  line emitted from hydrogen alone, xenon-hydrogen mixture (90/10)%, and helium-hydrogen mixture (90/10)% microwave discharge plasmas maintained in the microwave discharge cell shown in Figure 1 was measured with a high resolution visible spectrometer capable of a resolution of  $\pm 0.006 \text{ nm}$  [10-11]. In this case, the total pressure was 1 Torr, and the input power to the plasma was set at 40 W.

$T_e$  was measured on 0.1 Torr microwave plasmas of helium or hydrogen alone, xenon-hydrogen mixture (90/10%), and helium-hydrogen mixture (90/10%) using the ratio of the intensity  $I$  of two lines in two quantum states. For example,  $T_e$  was measured on helium from the ratio of the intensity of the He 501.6 nm (upper quantum level  $n=3$ ) line to that of the He 492.2 nm ( $n=4$ ) line as described by Griem [12], and  $T_e$  was measured on hydrogen alone plasmas from their Balmer line intensities. The visible spectrum 400–560 nm was recorded with a normal

incidence EUV spectrometer using a PMT and a sodium salicylate scintillator as described previously [10-11].

The electron density was determined using a Langmuir probe according to the method given previously [13].

### III. RESULTS

#### ToF-SIMS

The positive ion ToF-SIMS spectra of a cleaned commercial silicon wafer before and after being coated with a carbon film are shown in Figures 2 and 3, respectively. The positive ion spectrum of the control was dominated by  $Si^+$ , oxides  $Si_xO_y^+$ , and hydroxides  $Si_x(OH)_y^+$ ; whereas, that of the carbon film sample contained no silicon containing fragments. Rather, a large  $H^+$  peak and trace hydrocarbon fragments  $C_xH_y^+$  were observed. The  $m/e=69$  peak was due to the  $Ga^+$ .

The negative ion ToF-SIMS spectra of a cleaned commercial silicon wafer before and after being coated with a carbon film are shown in Figures 4 and 5, respectively. The control spectrum was dominated by oxide ( $O^-$ ) and hydroxide ( $OH^-$ ); whereas, spectrum of the carbon film was dominated by hydride ion ( $H^-$ ) and carbon ion ( $C^-$ ). Very little oxide ( $O^-$ ) or hydroxide ( $OH^-$ ) was observed. An exceptional feature was the multimeric carbon clusters  $C_x^-$  at  $m/e=12,24,36,48,60,72,96,108,120$ .

#### XPS

A survey spectrum was obtained over the region  $E_b = 0$  eV to 1200 eV. The primary element peaks allowed for the determination of all of the elements present. The XPS survey scan of a cleaned commercial silicon wafer before and after being coated with a carbon film are shown in Figures 6 and 7, respectively. The major peaks identified in the XPS spectrum of the control sample were  $O 1s$  at 533.0 eV, trace  $C 1s$  at 284.6 eV, dominant  $Si 2s$  at 152.4 eV and  $Si 2p_{3/2}$  at 101.9 eV. Whereas, the carbon film sample comprised only carbon and trace silicon and oxygen contamination as indicated by the trace  $O 1s$  peak at 532.9 eV, the trace  $Si 2s$  at 153.2 eV and  $Si 2p_{3/2}$  at 102.2 eV, and the dominant  $C 1s$  peak at 284.6 eV.



The high resolution XPS spectra (0-35 eV) of the valence band region of (a) single crystal diamond, (b) diamond film, (c) glassy carbon, (d) pyrolytic graphite, (e) mineral graphite, and (f) HDLC are shown in Figure 8 [14]. The corresponding XPS spectrum of the carbon film sample is shown in Figure 9. The film had a sharp peak at 13.2 eV and a broad peak at 17.4 eV which matched the peak energies of single crystal diamond rather than that of the other forms of carbon which were observed at higher binding energies. No  $O 2s$  peak was also observed in the region of 23 eV as shown in Figure 9.

The high resolution XPS spectra (280-340 eV) of the  $C 1s$  energy loss region of (a) single crystal diamond, (b) diamond film, (c) glassy carbon, (d) pyrolytic graphite, (e) mineral graphite, and (f) HDLC are shown in Figure 10 [14]. The corresponding XPS spectrum of the carbon film sample is shown in Figure 11. Single crystal diamond, diamond film, and HDLC have an energy loss feature which begins at about 290 eV which is at a higher energy than that of the other possible forms of carbon as shown in Figure 10. The closest match to the shape of the energy loss feature of the carbon film is single crystal diamond to which the film was assigned.

### Raman

The Raman spectrum of the corresponding region of the diamond film is shown in Figure 12. The peak positions, full-width-half-maximum (FWHM), and peak areas were calculated by Gaussian curve fitting the baseline corrected spectrum. The diamond band was observed at  $1323.5 \text{ cm}^{-1}$ , with a FWHM of  $19.6 \text{ cm}^{-1}$ . The diamond peak width of less than  $20 \text{ cm}^{-1}$  identified the film as having single crystal diamond [15]. In addition to the diamond band, the D-band, G-band of diamond-like carbon (DLC), and G-band of graphite were observed at  $1327.0 \text{ cm}^{-1}$  with a FWHM of  $76 \text{ cm}^{-1}$ ,  $1484.0 \text{ cm}^{-1}$  with a FWHM of  $130.2 \text{ cm}^{-1}$ , and  $1591.6 \text{ cm}^{-1}$  with a FWHM of  $46.5 \text{ cm}^{-1}$ , respectively.

The ratio of the areas of the diamond peak to G-band of graphite,  $\frac{I_D}{I_G}$ , is considered an indirect measure of carbon  $\frac{sp^3}{sp^2}$  bonding ratio. The ratio  $\frac{I_D}{I_G}$  was 0.73. The Raman spectrum confirmed the XPS results that

the film comprised diamond. Based on quantitative studies [16-17], we estimate that the diamond composition of the films was well over 50%.

### XRD

The X-ray Diffraction (XRD) pattern of the diamond film for  $2\theta = 10^\circ$  to  $100^\circ$  is shown in Figure 13. The dominant peaks were due to silicon of the substrate. Diamond peaks were observed at  $2\theta = 43.9^\circ$  (111) and  $75.3^\circ$  (220) [18-19]. Additional peaks other than silicon and diamond corresponded to DLC.

### Line broadening and $T_e$ measurements

The Doppler-broadened line shape for atomic hydrogen has been studied on many sources such as hollow cathode [20-21] and rf [22-23] discharges. The method of Videnovic et al. [20] was used to calculate the energetic hydrogen atom densities and energies from the width of the 656.3 nm Balmer  $\alpha$  line emitted from microwave discharge plasmas of hydrogen compared with each of xenon-hydrogen (90/10%) and helium-hydrogen (90/10%) as shown in Figures 14-15, respectively. Gigosos et al. [24] have published a literature review of this method. The average helium-hydrogen Doppler half-width of  $0.52 \pm 5\% \text{ nm}$  was not appreciably changed with pressure. The corresponding energy of 180-210 eV and the number densities of  $5 \times 10^{14} \pm 20\% \text{ atoms/cm}^3$ , depending on the pressure, were significant compared to only  $\approx 3 \text{ eV}$  and  $7 \times 10^{13} \pm 20\% \text{ atoms/cm}^3$  for pure hydrogen, even though 10 times more hydrogen was present. Xenon did not serve as a catalyst, and the plasma was much less energetic. Xenon-hydrogen showed no excessive broadening corresponding to an average hydrogen atom temperature of  $\approx 3 \text{ eV}$ , and the atom density was also low,  $3 \times 10^{13} \pm 20\% \text{ atoms/cm}^3$ .

Similarly, the average electron temperature for helium-hydrogen plasma was  $28,000 \pm 5\% \text{ K}$ . Whereas, the corresponding temperature of helium alone was only  $6800 \pm 5\% \text{ K}$ , hydrogen alone was  $5500 \pm 5\% \text{ K}$ , and xenon-hydrogen was  $6500 \pm 5\% \text{ K}$ .

We have assumed that Doppler broadening due to thermal motion was the dominant source to the extent that other sources may be neglected. This assumption was confirmed when each source was considered. In general, the experimental profile is a convolution of two

Doppler profiles, an instrumental profile, the natural (lifetime) profile, Stark profiles, Van der Waals profiles, a resonance profile, and fine structure. The electron density recorded with a Langmuir probe was five orders of magnitude too low for detectable Stark broadening, and the contribution from each remaining source was determined to be below the limit of detection [10-11].

#### IV. DISCUSSION

Silicon substrates were coated by the reaction product of a low pressure  $He$  (90-70%)/ $H_2$  (10-30%)/ $CH_4$  (1-10%) microwave discharge plasma. The ToF-SIMS of the carbon film showed carbon clusters, and the XPS matched single crystal diamond which was confirmed by the Raman diamond peak at  $1323.5\text{ cm}^{-1}$  with a FWHM of less than  $20\text{ cm}^{-1}$ . Diamond is proposed to form from  $CH_4$  by the catalytic reaction of  $He^+$  with atomic hydrogen which forms an energetic plasma which was measured to have extraordinarily fast H.

In the previously developed  $CH_4$ - $H_2$ -system and variations thereof, diamond formation occurs within a small domain about the  $C-H-O$  tie line. Stringent conditions of a large excess of hydrogen, diamond seeding, and an elevated temperature are required. Similarly, in the  $CO_2/CH_4$  system, diamond only formed within a range of a few percent from a 50/50% mixture. We observed for the first time that diamond was very reproducibly formed from a  $CH_4$  carbon source with a helium-hydrogen plasma without the requirements of diamond seeding, an elevated temperature, or an excess of hydrogen, or any particular former set of stringent conditions. Thus, a dramatic breakthrough in thin film diamond deposition has been shown.

The mechanism may be based on energetic hydrogen formed in the plasma reaction. Diamond and DLC are metastable materials; thus, continuous bombardment of the surface with energetic species that produce thermal and pressure spikes at the growth surface is required for deposition of diamond, DLC, and related films [25]. By quenching a beam of  $C^+$  ions accelerated in an ultrahigh vacuum to a negatively biased substrate, Aisenberg and Chabot [26] were able to deposit DLC films for the first time. Rather than resulting in commercially useful

processes, subsequently developed beam-type and sputtering production methods are essentially used for research. Exemplary methods discussed by Grill and Myerson [27] are single low-energy beams of carbon ions, dual ion beams of carbon and argon, ion plating, RF sputtering or ion-beam sputtering from carbon/graphite targets, vacuum-arc discharges, and laser ablation. Using sputter deposition, amorphous DLC coatings can be prepared at low temperature due to high ion bombardment during the deposition of carbon. The absence of ion bombardment during carbon deposition leads to soft, conductive carbon films with no diamond-like properties. It has been shown that films with diamond-like properties are produced at ion energies of about 100 eV [28-29].

Energetic species such as fast H formed in the helium-hydrogen microwave plasma that showed extraordinary Balmer  $\alpha$  line broadening corresponding to an average hydrogen atom temperature of 180-210 eV may be the basis of the formation of the diamond film from  $CH_4$ . Without diamond seeding, production of single crystal diamond films on heterogeneous substrates was achieved under relatively low temperature, nonstringent conditions.

### ACKNOWLEDGMENTS

Thanks to A. Miller of Lehigh University for XPS analysis and very useful discussions, and V. Pajcini of Charles Evans & Associates for Raman analysis and useful discussions.

### REFERENCES

1. P. W. May, "Diamond thin films: a 21 st-century material", Phil. Trans. R. Soc. Lond. A, Vol. 358, (2000), pp. 473-495.
2. J. O. Orwa, S. Praver, D. N. Jamieson, J. L. Peng, J. C. McCallum, K. W. Nugent, Y. J. Li, L. A. Bursill, "Diamond nanocrystals formed by direct implantation of fused silica with carbon", Journal of Applied Physics, Vol. 90, No. 6, (2001), pp. 3007-3018.
3. M. A. Elliott, P. W. May, J. Petherbridge, S. M. Leeds, M. N. R. Ashfold, W. N. Wang, "Optical emission spectroscopic studies of microwave

- enhanced diamond CVD using  $CH_4/CO_2$  plasmas", *Diamond and Related Materials*, Vol. 9, (2000), pp. 311-316.
4. J. R. Petherbridge, P. W. May, S. R. J. Pearce, K. N. Rosser, M. N. R. Ashfold, "Low temperature diamond growth using  $CO_2/CH_4$  plasmas: Molecular beam mass spectroscopy and computer simulation investigations", *Journal of applied Physics*, Vol. 89, No. 2, Jan. 15, (2001), pp. 1484-1492.
  5. J. Petherbridge, P. W. may, S. R. J. Pearce, K. N. Rosser, M. N. R. Ashfold, "Molecular beam mass spectrometry investigations of low temperature diamond growth using  $CO_2/CH_4$  plasmas", *Diamond and Related Materials*, Vol. 10, (2001), pp. 393-398.
  6. P. K. Bachmann, D. Leers, H. Lydtin, D. U. Wiechert, *Diamond and Related Materials*, Vol. 1, No. 1, (1991), p. 1.
  7. P. K. Bachmann, H. G. Hagemann, H. Lade, D. Leers, F. Picht, D. U. Wiechert, *Mater. Res. Soc. Proc.*, Vol. 339, (1994), p. 267.
  8. R. L. Mills, B. Dhandapani, J. He, "Highly Stable Amorphous Silicon Hydride", *J of Materials Research*, submitted.
  9. J. H. D. Rebello, D. L. Straub, V. V. Subramaniam, "diamond growth from a  $CO/CH_4$  mixture by laser excitation of  $CO$ : Laser excited chemical vapor deposition", *J. Appl. Phys.*, Vol. 72, No. 3, (1992), pp. 1133-1136.
  10. R. L. Mills, P. Ray, "Substantial Changes in the Characteristics of a Microwave Plasma Due to Combining Argon and Hydrogen", *New Journal of Physics*, [www.njp.org](http://www.njp.org), Vol. 4, (2002), pp. 22.1-22.17.
  11. R. L. Mills, P. Ray, B. Dhandapani, J. He, "Comparison of Excessive Balmer  $\alpha$  Line Broadening of Glow Discharge and Microwave Hydrogen Plasmas with Certain Catalysts", *J. of Applied Physics*, submitted.
  12. H. R. Griem, *Principles of Plasma Spectroscopy*, Cambridge University Press, (1987).
  13. D. Barton, J. W. Bradley, D. A. Steele, and R. D. Short, "investigating radio frequency plasmas used for the modification of polymer surfaces," *J. Phys. Chem. B*, Vol. 103, (1999), pp. 4423-4430.
  14. Provided by A. Miller, Zettlemoyer Center for Surface Studies, Sinclair Laboratory, Lehigh University Bethlehem, PA.
  15. M. G. Donato, G. Faggio, M. Marinelli, G. Messina, E. Milani, A. Paoletti, S. Santangelo, A. Tucciarone, G. Verona Rinati, *Diamond and Related Materials*, Vol. 10, (2001), pp. 1788-1793.

16. S. M. Leeds, T. J. Davis, P. W. May, C. D. O. Pickard, M. N. R. Ashfold, "Use of different wavelengths for analysis of CVD diamond by laser Raman Spectroscopy", *Diamond and Related Materials*, Vol. 7, (1998), pp. 233-237.
17. K. W. R. Gilkes, S. Praver, K. W. Nugent, J. Robertson, H. S. Sands, Y. Lifshitz, X. Shi, "Direct quantitative detection of the  $sp^3$  bonding in diamond-like carbon films using ultraviolet and visible Raman spectroscopy", *Journal of Applied Physics*, Vol. 87, No. 10, (2000), pp. 7283-7289.
18. P. D. Ownby, X. Yang, J. Liu, *J. Am. Ceram. Soc.*, Vol. 75, (1992), p. 1876.
19. J. Thewlis, A. R. Davey, *Philos. Mag.*, Part B, Vol. 1, (1956), p. 409.
20. I. R. Videnovic, N. Konjevic, M. M. Kuraica, "Spectroscopic investigations of a cathode fall region of the Grimm-type glow discharge", *Spectrochimica Acta*, Part B, Vol. 51, (1996), pp. 1707-1731.
21. S. Alexiou, E. Leboucher-Dalimier, "Hydrogen Balmer- $\alpha$  in dense plasmas", *Phys. Rev. E*, Vol. 60, No. 3, (1999), pp. 3436-3438.
22. S. Djurovic, J. R. Roberts, "Hydrogen Balmer alpha line shapes for hydrogen -argon mixtures in a low-pressure rf discharge", *J. Appl. Phys.*, Vol. 74, No. 11, (1993), pp. 6558-6565.
23. S. B. Radovanov, K. Dzierzega, J. R. Roberts, J. K. Olthoff, "Time-resolved Balmer-alpha emission from fast hydrogen atoms in low pressure, radio-frequency discharges in hydrogen", *Appl. Phys. Lett.*, Vol. 66, No. 20, (1995), pp. 2637-2639.
24. M. A. Gigosos, V. Cardenoso, "New plasma diagnosis tables of hydrogen Stark broadening including ion dynamics", *J. Phys. B: At. Mol. Opt. Phys.*, Vol. 29, (1996), pp. 4795-4838.
25. C. Weissmantel, *Thin Films from Free Atoms and Molecules*, K. J. Klabunde, Ed., Academic Press, Inc., New York, (1985), p. 153.
26. S. Aisenberg, R. Chabot, *J. Appl. Phys.*, Vol. 42, (1971), p. 2953.
27. A. Grill, B. Meyerson, *Synthetic Diamond: Emerging CVD Science and Technology*, K. E. Spear and J. P. Dismukes, Eds., John Wiley & Sons, Inc., New York, (1994), p. 91.
28. J. Ishikawa, K. Ogawa, K. Miyata, T. Takagi, *Nucl. Instrum. Methods*, Vol. B21, (1987), p. 205.

29. F. Rossi, B. Andre, in Proc. IP AT 1991, Brussels, CEP Consultants, Edinburgh, UK, (1991), p. 43.

## Figure Captions

Figure 1. The experimental set up comprising a microwave discharge cell operated under flow conditions.

Figure 2. The positive ion ToF-SIMS spectra ( $m/e = 0-800$ ) of a noncoated cleaned commercial silicon wafer.

Figure 3. The positive ion ToF-SIMS spectra ( $m/e = 0-200$ ) of a cleaned commercial silicon wafer coated by reaction of a helium-hydrogen plasma with  $CH_4$  as the source of C that showed a large  $H^+$  peak and trace hydrocarbon fragments  $C_xH_y^+$ .

Figure 4. The negative ion ToF-SIMS spectrum ( $m/e = 0-800$ ) of a noncoated cleaned commercial silicon wafer.

Figure 5. The negative ion ToF-SIMS spectrum ( $m/e = 0-200$ ) of a cleaned commercial silicon wafer coated by reaction of a helium-hydrogen plasma with  $CH_4$  as the source of C that was dominated by hydride ion ( $H^-$ ) and carbon ion ( $C^-$ ). Very little oxide ( $O^-$ ) or hydroxide ( $OH^-$ ) was observed. An exceptional feature was the multimeric carbon clusters  $C_x^-$  at  $m/e = 12, 24, 36, 48, 60, 72, 96, 108, 120$ .

Figure 6. The XPS survey scan of a cleaned commercial silicon wafer. Only silicon, oxygen, and trace carbon contamination were observed.

Figure 7. The XPS survey scan of a cleaned commercial silicon wafer coated by reaction of a helium-hydrogen plasma with  $CH_4$  as the source of C. Only carbon and trace silicon and oxygen contamination were observed.

Figure 8. High resolution XPS spectra (0-35 eV) of the valence band region of (a) single crystal diamond, (b) diamond film, (c) glassy carbon, (d) pyrolytic graphite, (e) mineral graphite, and (f) HDLC.

Figure 9. High resolution XPS spectra (0-35 eV) of the valence band region of a cleaned commercial silicon wafer coated by reaction of a helium-hydrogen plasma with  $CH_4$  as the source of C that showed features that matched single crystal diamond.

Figure 10. High resolution XPS spectra (280-340 eV) of the C 1s energy loss region of (a) single crystal diamond, (b) diamond film, (c) glassy carbon, (d) pyrolytic graphite, (e) mineral graphite, and (f) HDLC.



Figure 11. High resolution XPS spectrum (280-340 eV) of the C 1s energy loss region of a cleaned commercial silicon wafer coated by reaction of a helium-hydrogen plasma with  $CH_4$  as the source of C that showed features that matched single crystal diamond.

Figure 12. The Raman spectrum recorded on the diamond film. The diamond band, D-band, G-band of DLC, and G-band of graphite were observed at  $1323.5\text{ cm}^{-1}$ ,  $1327.0\text{ cm}^{-1}$ ,  $1484.0\text{ cm}^{-1}$  and  $1591.6\text{ cm}^{-1}$ , respectively. The  $19.6\text{ cm}^{-1}$  FWHM of the diamond peak is characteristic of and identified the film as having single crystal diamond.

Figure 13. The X-ray Diffraction (XRD) pattern of a diamond film for  $2\theta = 10^\circ$  to  $100^\circ$ . The dominant peaks were due to silicon of the substrate. Diamond peaks were observed at  $2\theta = 43.9^\circ$  (111) and  $75.3^\circ$  (220).

Figure 14. The 656.3 nm Balmer  $\alpha$  line width recorded with a high resolution ( $\pm 0.006\text{ nm}$ ) visible spectrometer on a xenon-hydrogen (90/10%) and a hydrogen microwave discharge plasma. No line excessive broadening was observed corresponding to an average hydrogen atom temperature of 3-4 eV.

Figure 15. The 656.3 nm Balmer  $\alpha$  line width recorded with a high resolution ( $\pm 0.006\text{ nm}$ ) visible spectrometer on a helium-hydrogen (90/10%) and a hydrogen microwave discharge plasma. Significant broadening was observed corresponding to an average hydrogen atom temperature of 180-210 eV.

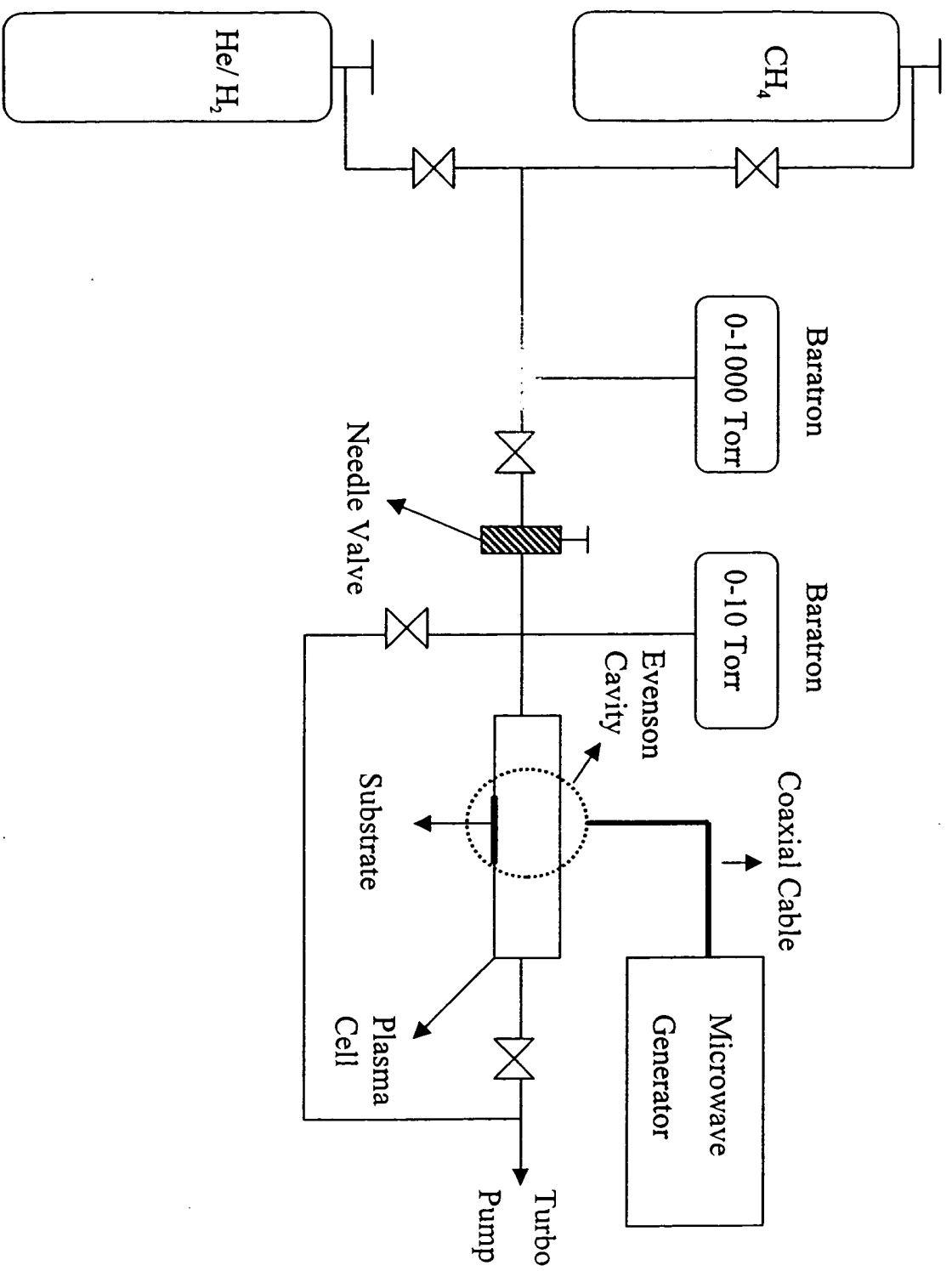


Fig. 1

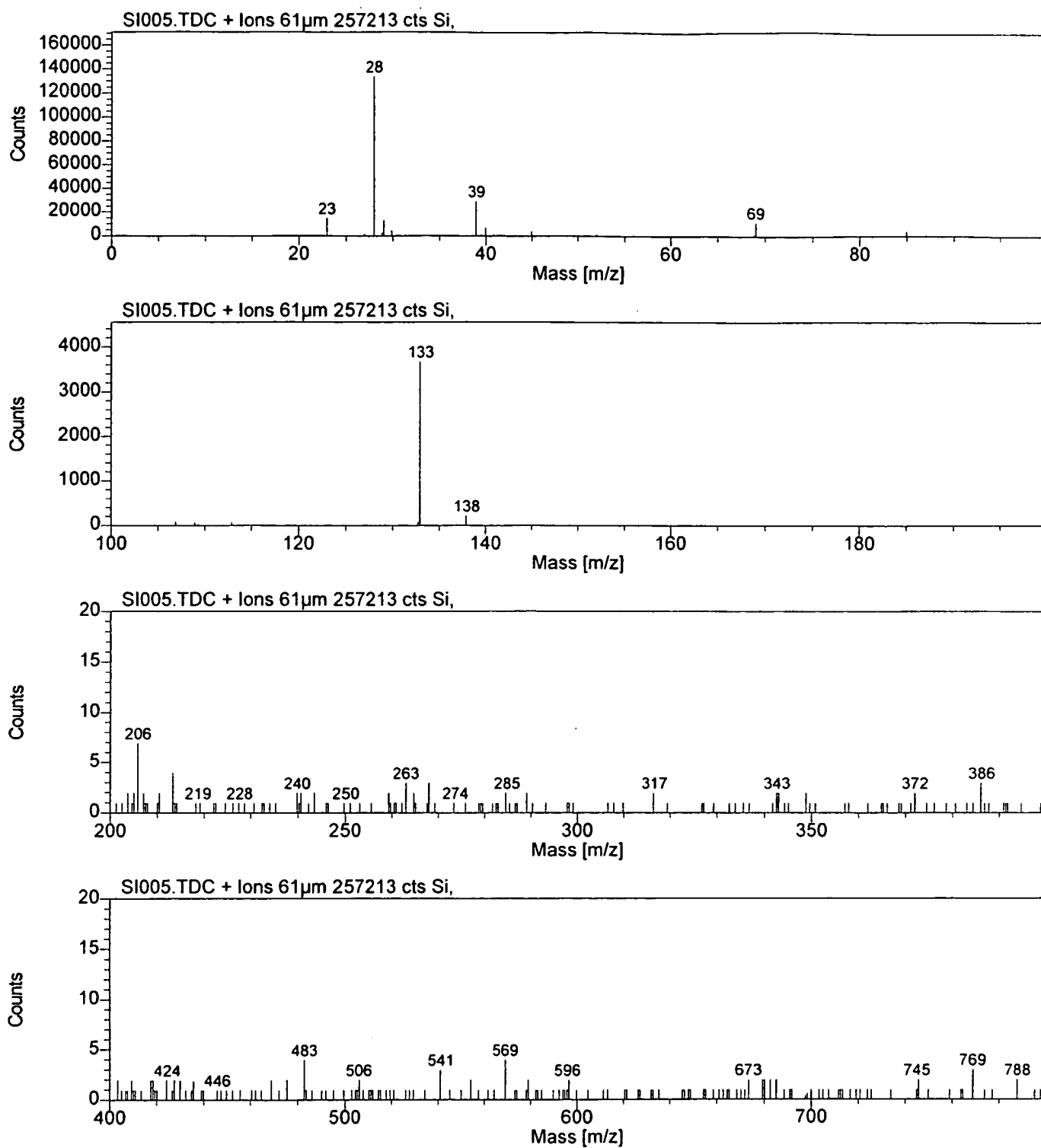


Fig. 2

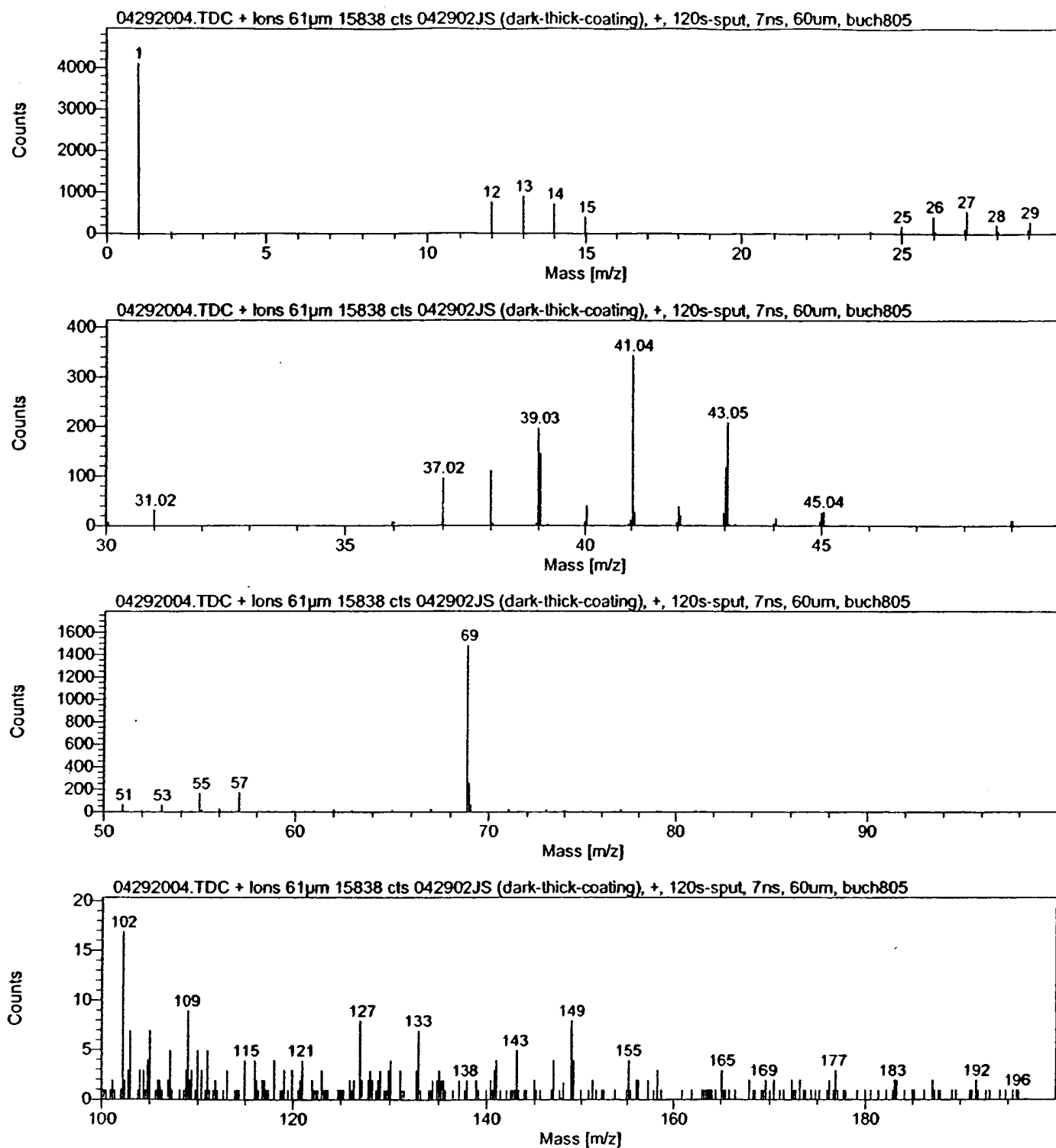


Fig. 3

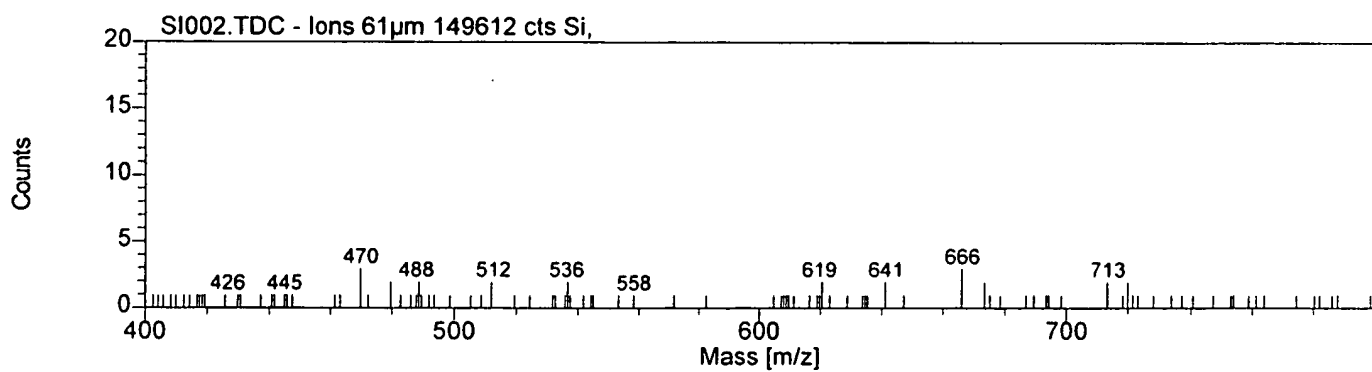
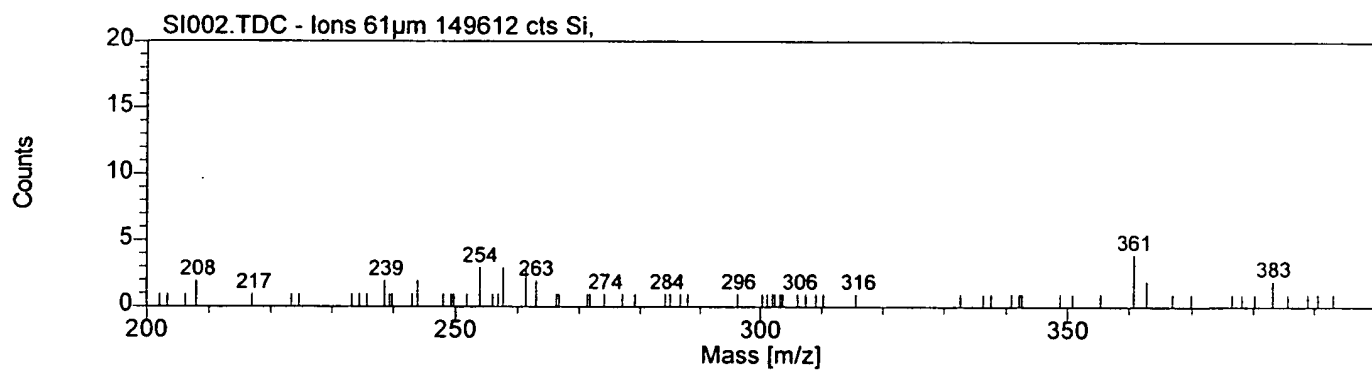
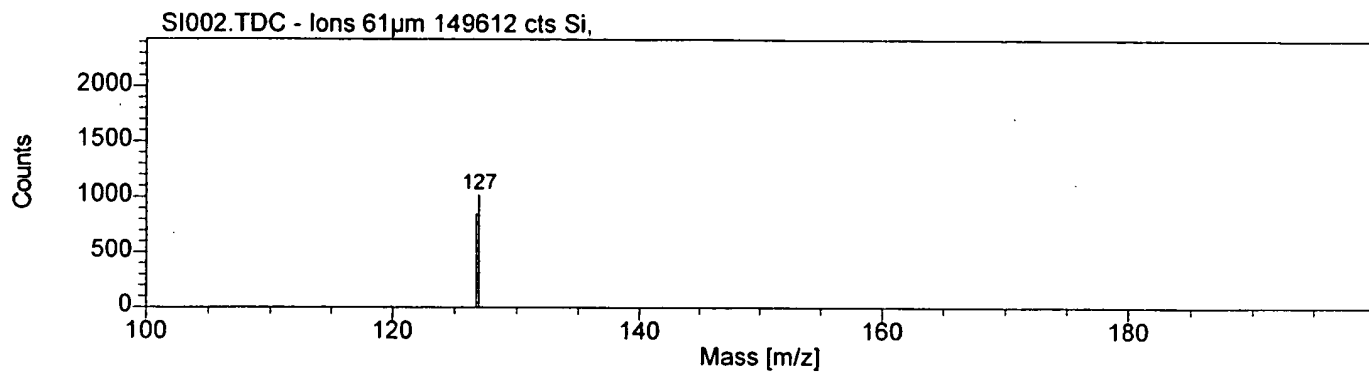
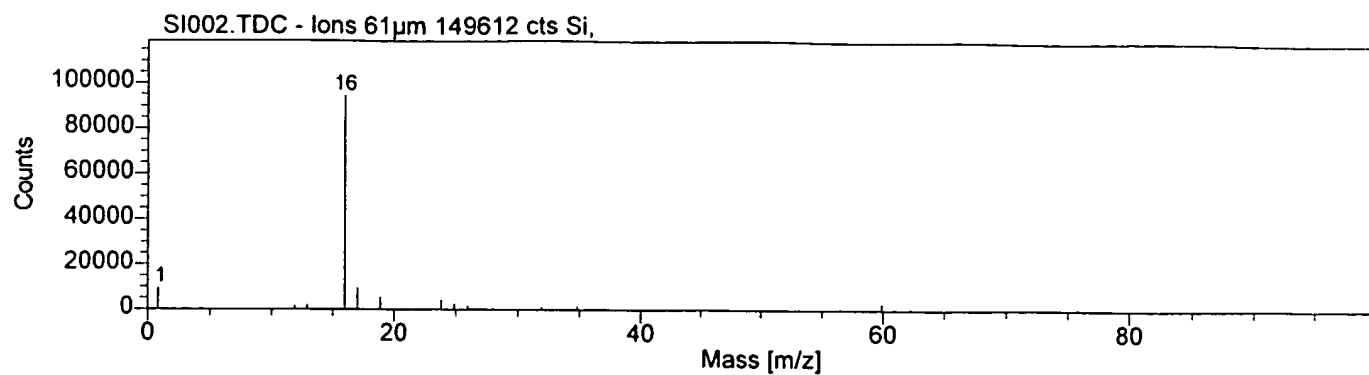


Fig. 4

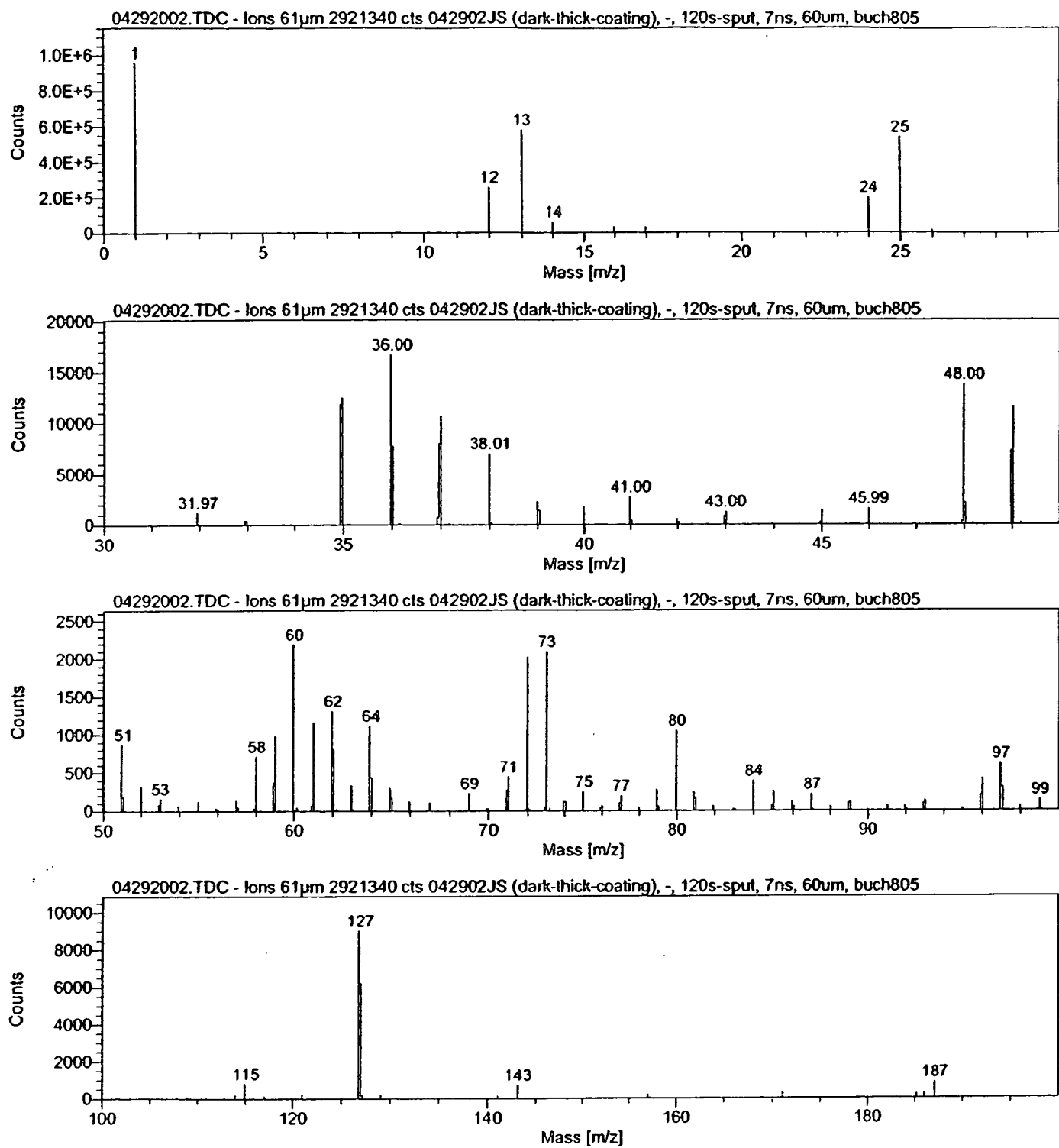


Fig. 5

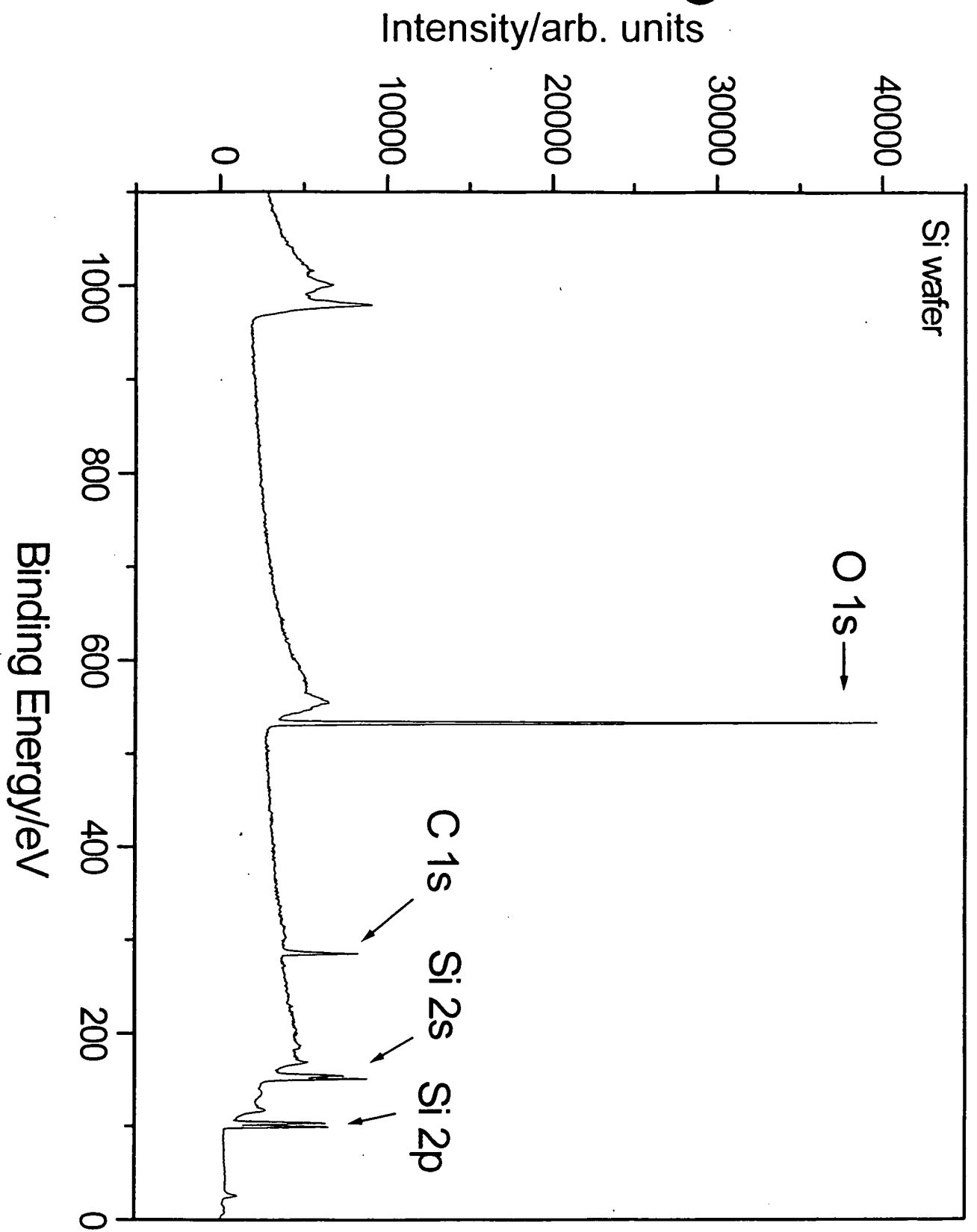


Fig. 6

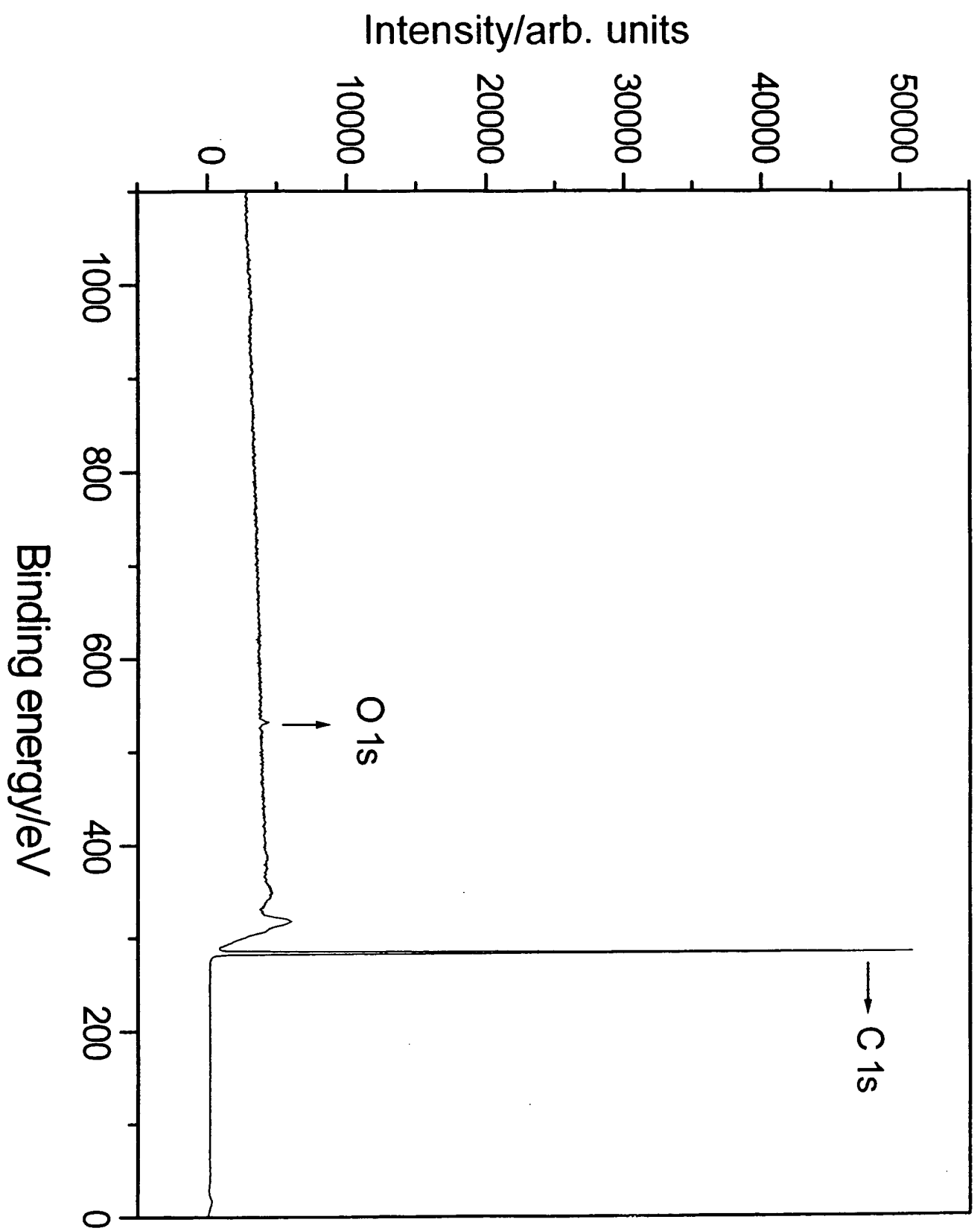


Fig. 7



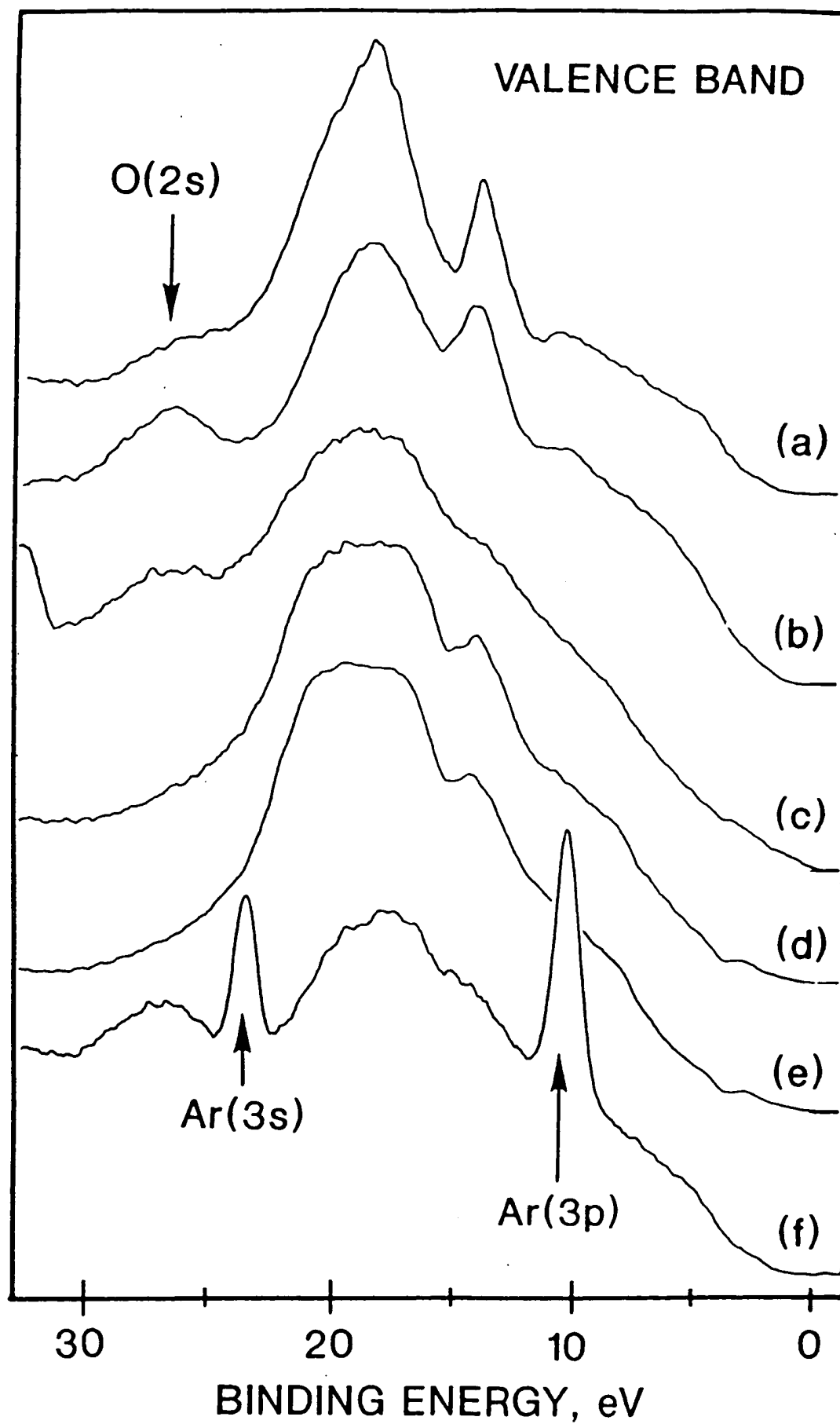


Fig. 8

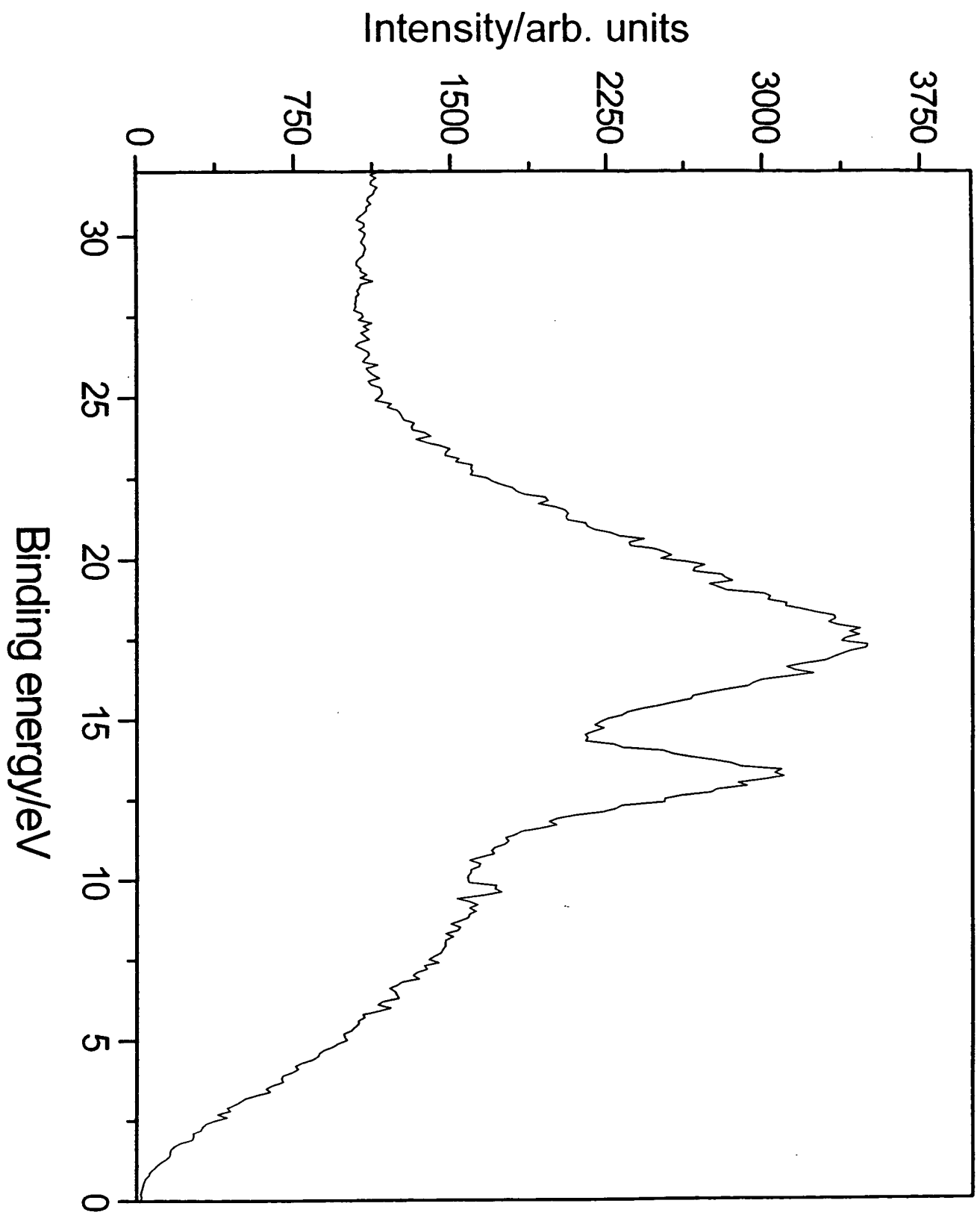


Fig. 9

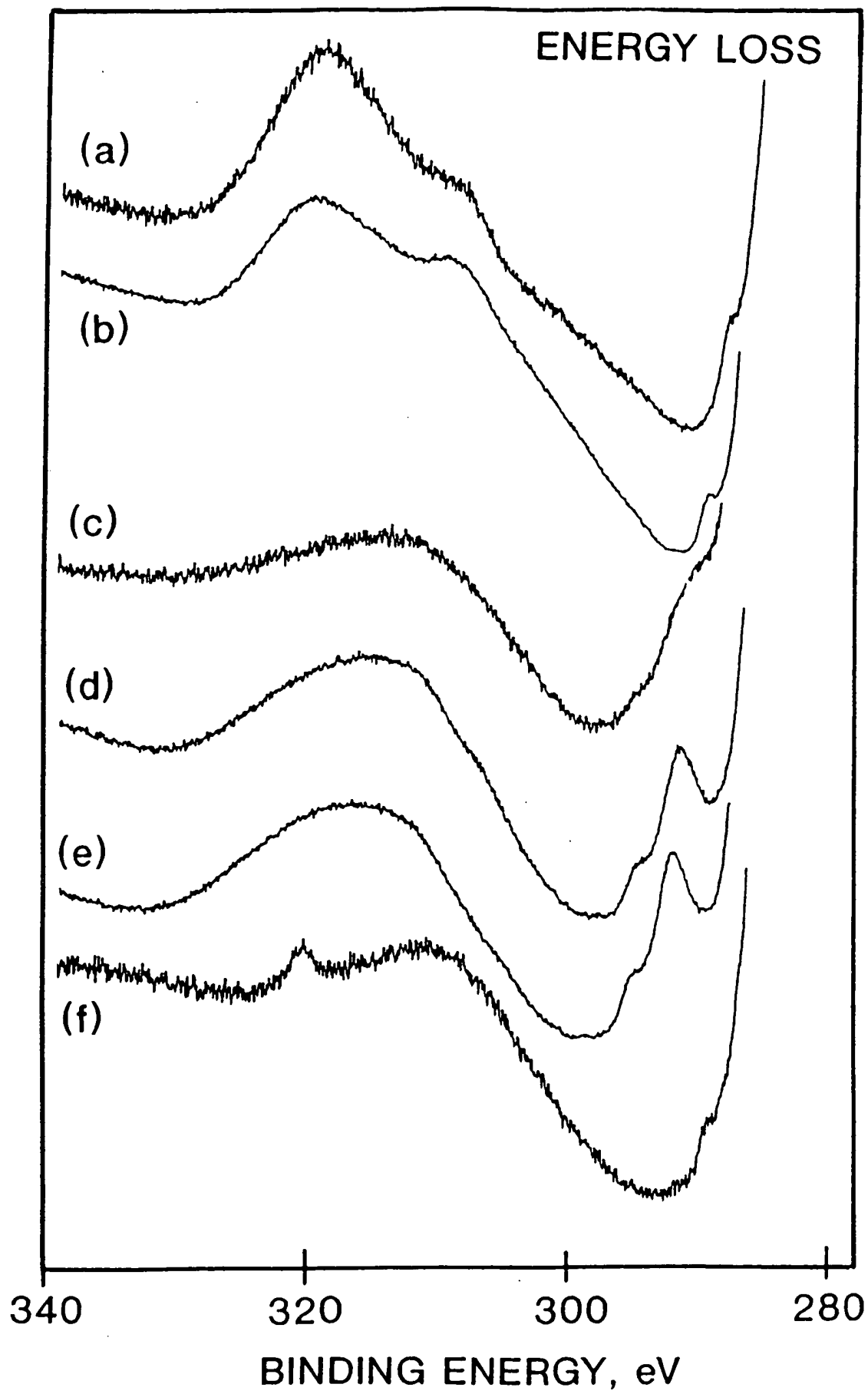


Fig. 10

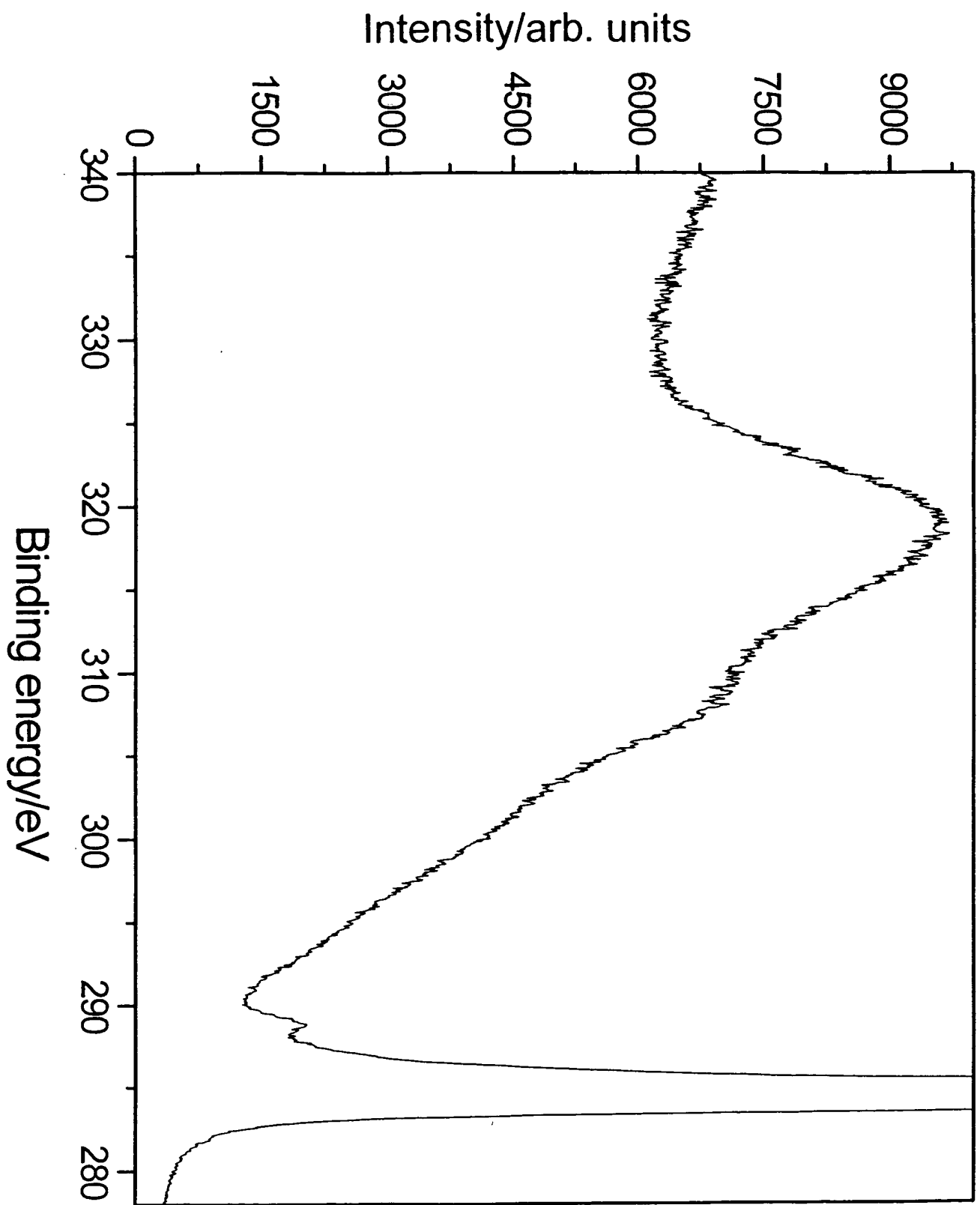


Fig. 11

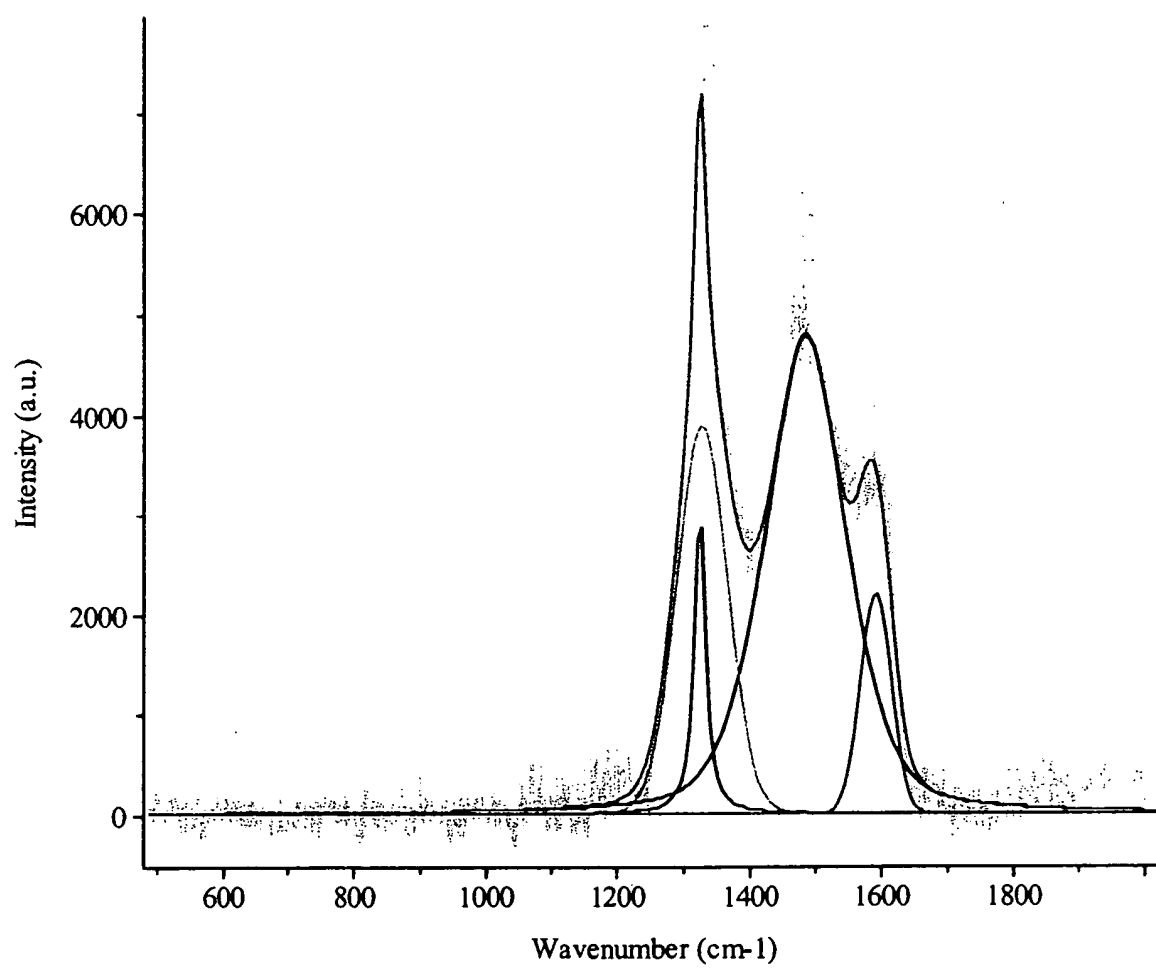


Fig. 12

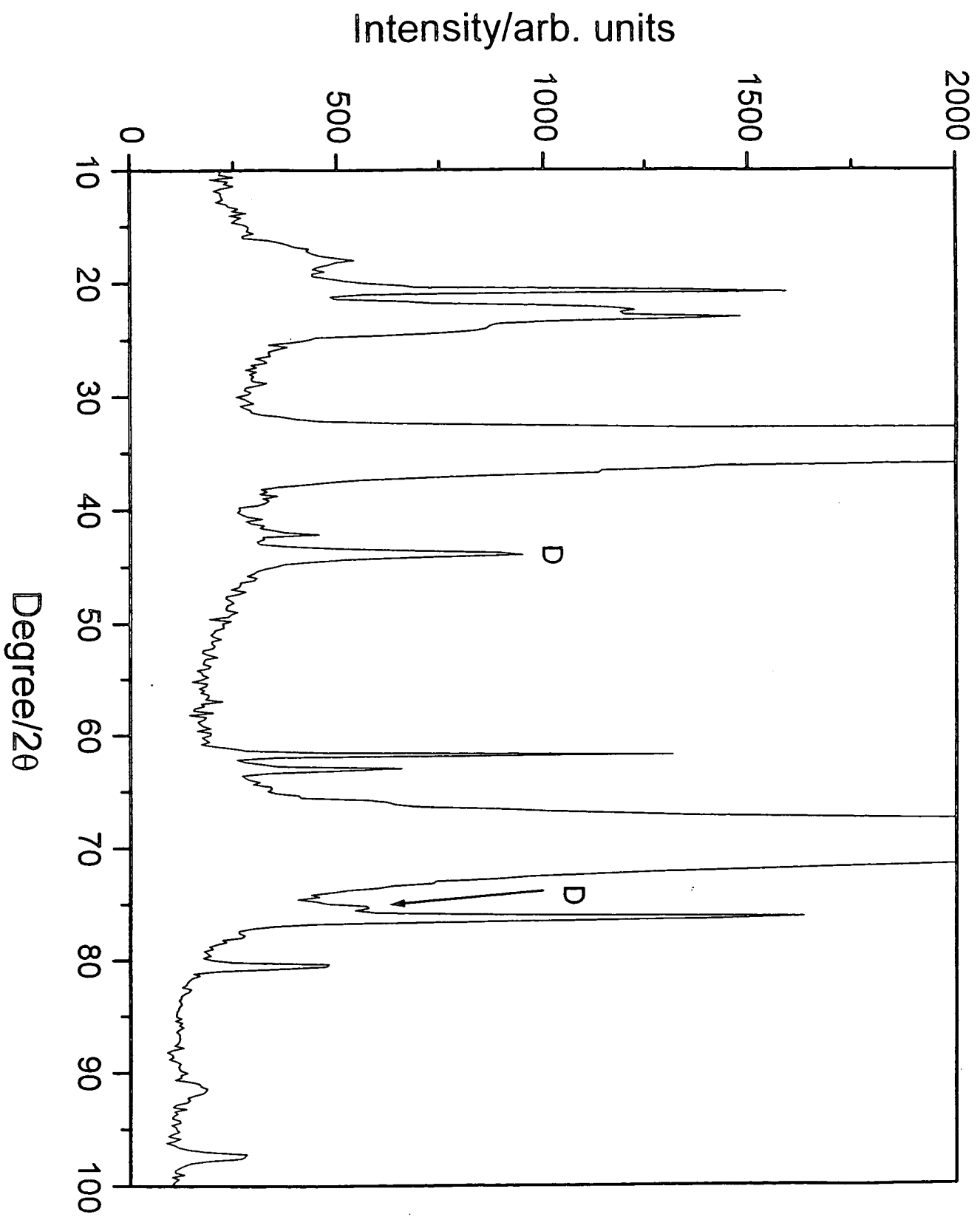


Fig. 13

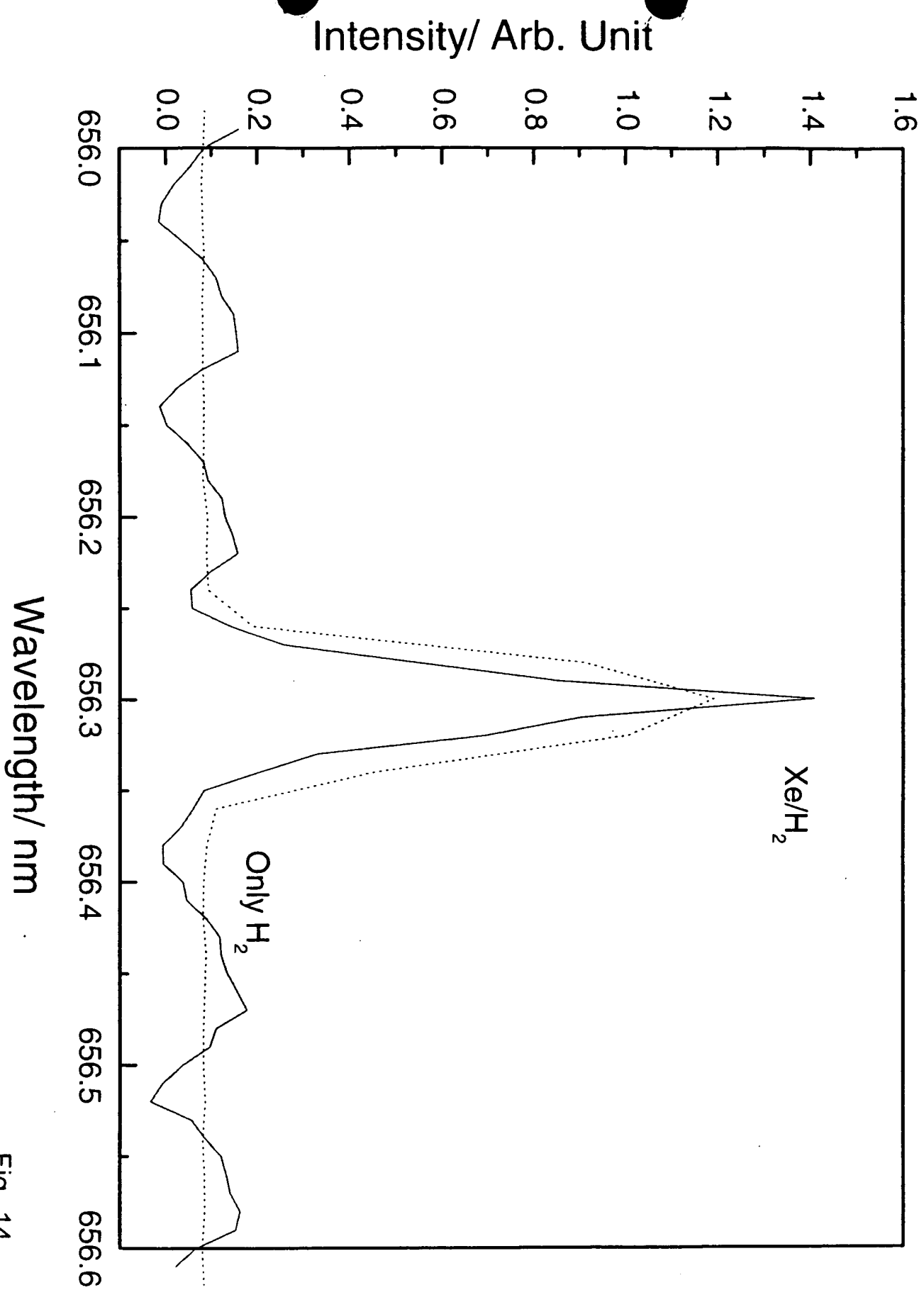


Fig. 14

Wavelength/ nm

Intensity/ Arb. Unit

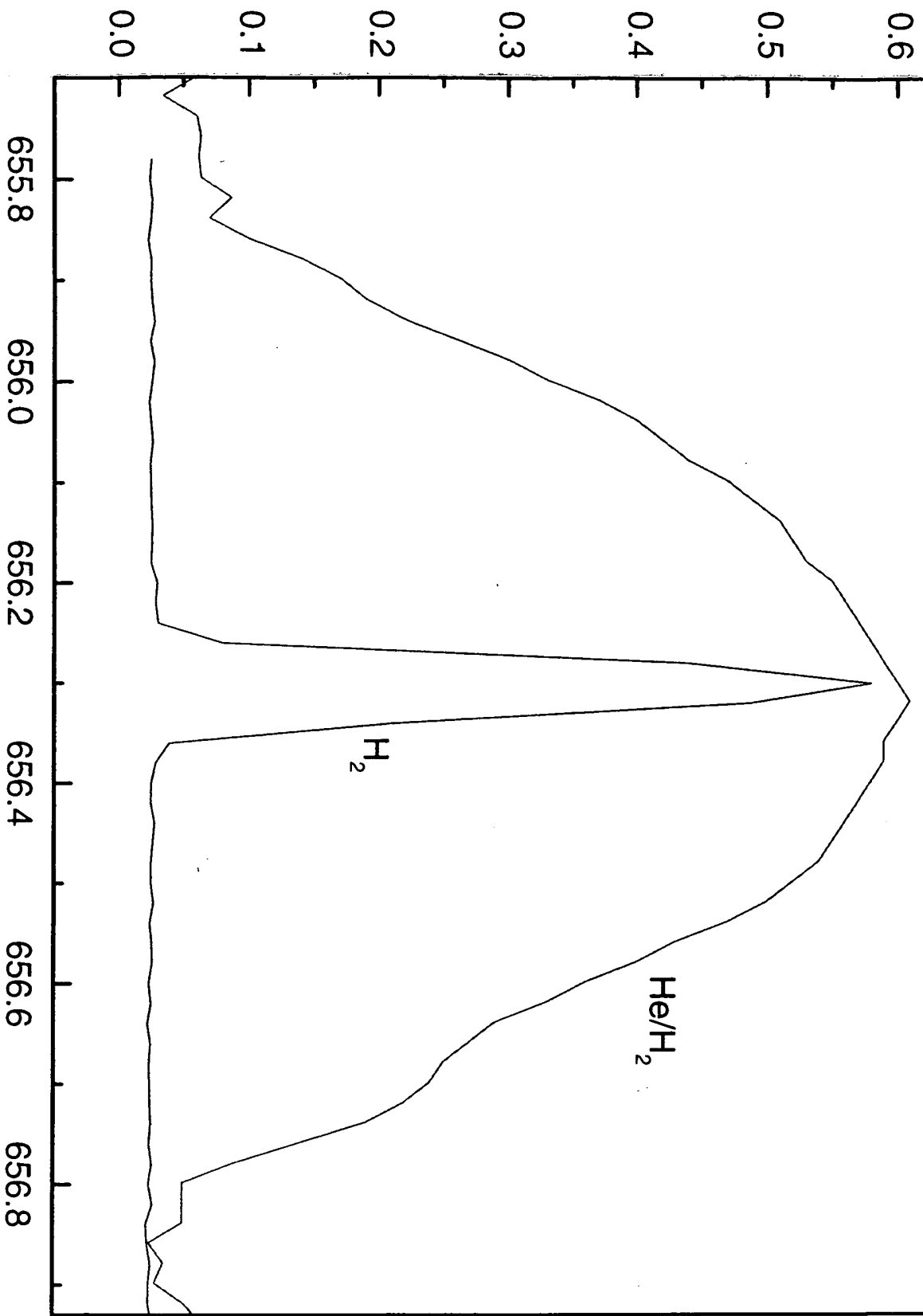


Fig. 15